# Calculating corner singularities by boundary integral equations

HUALIANG SHI[1,*], YA YAN LU[2], AND QIANG DU[3]

[1] Applied and Computational Mathematics Division, Beijing Computational Science Research Center, Beijing, 100193, China
[2] Department of Mathematics, City University of Hong Kong, Kowloon, Hong Kong
[3] Department of Applied Physics and Applied Mathematics, Columbia University, New York, NY10027, USA
[*] Corresponding author: shi.hualiang@csrc.ac.cn

Compiled May 12, 2017

**Accurate numerical solutions for electromagnetic fields near sharp corners and edges are important for nanophotonics applications that rely on strong near-fields to enhance light-matter interactions. For cylindrical structures, the singularity exponents of electromagnetic fields near sharp edges can be solved analytically, but in general the actual fields can only be calculated numerically. In this paper, we use a boundary integral equation method to compute electromagnetic fields near sharp edges, and construct the leading terms in asymptotic expansions based on numerical solutions. Our integral equations are formulated for rescaled unknown functions to avoid unbounded field components, and are discretized with a graded mesh and properly chosen quadrature schemes. The numerically found singularity exponents agree well with the exact values in all the test cases presented here, indicating that the numerical solutions are accurate.** 

***OCIS codes:*** *(000.4430) Numerical approximation and analysis; (050.1755) Computational electromagnetic methods.*

http://dx.doi.org/

## 1. INTRODUCTION

Electromagnetic fields around metallic nanoparticles and in subwavelength apertures or slits of metallic films are often many orders of magnitude more intense than the incident wave [1, 2]. Strong near-fields of well-designed plasmonic structures have important applications in biological and chemical sensing [2, 3], and can be used to enhance nonlinear optical effects, quantum optical effects, Raman scattering and other emission processes [1]. The local field enhancement in plasmonic structures is the result of localized surface plasmon resonances, but geometric features such as corners and edges also strongly influence the near-fields. To analyze the local field enhancement phenomenon and to study the numerous applications, it is clearly important to calculate the near-fields accurately. In particular, it is essential to study mathematically sharp corners and edges where electromagnetic fields exhibit singularities and tend to infinity.

For two-dimensional (2D) structures, the study of the singular behavior of electromagnetic fields near sharp edges has a long history. According to Meixner [4], the leading term in an asymptotic expansion of the transverse components of the electric field (perpendicular to the edge direction) is proportional to $\rho^{\tau-1}$, where $\rho$ is the distance to the edge and $\tau$ is the singularity exponent. Notice that $\tau$ is related to the local properties of the structure around the edge, and it can be calculated analytically by solving a transcendental equation. However, in general, the coefficient of the leading term cannot be determined analytically. Without the coefficient, the field near the edge is still unknown.

Standard numerical methods, such as the finite element method (FEM) with polynomial basis functions, can be used to calculate electromagnetic fields around corners and edges. It is relatively easy to obtain numerical solutions that appear to capture the divergent singular behavior near corners and edges, but the accuracy of the numerical solutions may be limited. In particular, the numerical solutions often fail to give the correct asymptotic behavior of the singular electromagnetic fields. Since the singularity exponent $\tau$ can be calculated analytically, special FEM and other numerical methods have been developed using basis functions with the exact singular behavior [5, 6]. These methods can accurately capture field singularities at corners and edges, but are somewhat complicated to implement, especially for three-dimensional (3D) problems.

For 2D structures that are invariant in a spatial direction, the boundary integral equation (BIE) method is one of the most effective methods. To compute singular electromagnetic fields near sharp edges, the BIE method can also use special basis functions with the exact singularity [7–9]. Marx [10, 11] first used BIE methods without special basis functions to calculate

the near fields for a dielectric wedge. More recently, Disfani *et al.* [12] studied the near fields for plasmonic wedges using the same BIE formulation. In principle, if the numerical solutions are sufficiently accurate, one can reconstruct the singularity exponent $\tau$ and find the coefficient of the leading term. The numerical solutions of [10–12] exhibit qualitative agreement with the leading term of the asymptotic expansion, but it appears that they are not sufficiently accurate for reconstructing $\tau$. In principle, it is always possible to increase the accuracy by discretizing the BIEs with more points, and calculate the field to extreme proximity of the edge. In fact, the calculations reported in [11] have been carried out for the field down to a distance as small as $10^{-10}\lambda$ to the edge, where $\lambda$ is the incident wavelength, but the agreement between the calculated field and the leading asymptotic term is still not very good.

In this paper, we use a simple BIE formulation with a scaled unknown function, a graded mesh and two different discretization schemes to study scattering problems of cylindrical structures with sharp edges. Unlike the BIE methods developed in [7–9], our method is purely numerical, involves only discretization parameters, and does not require the knowledge of the singularity exponent. Based on the numerical solutions, we reconstruct the exponent $\tau$ and calculate the coefficient of the leading term. In all cases, the numerically reconstructed values of $\tau$ have at least two correct significant digits. It should be emphasized that the improved accuracy is not a result of simply using more discretization points, instead it comes from the improved numerical techniques for discretizing the properly reformulated BIEs. In fact, we are able to calculate the electromagnetic fields down to distance as small as $10^{-16}\lambda$ to the edge, at a moderate computational cost associated with only about a few hundreds total number of discretization points.

## 2. CORNER SINGULARITIES

We consider infinitely-long cylinders with axes in the $z$ direction and cross sections in the $xy$ plane, where $\{x, y, z\}$ is a Cartesian coordinate system. For simplicity, we assume the cross section has only one corner corresponding to the sharp edge of the cylinder, and introduce a polar coordinate system $\{\rho, \theta\}$ with the origin at the corner point. Two examples are shown in Fig. 1,

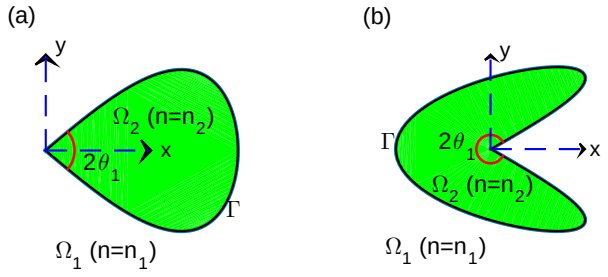


**Fig. 1.** Cross sections of two infinitely-long cylinders.

where $\Omega_2$ corresponds to the cross section of the cylinder, $2\theta_1$ is the inner angle of $\Omega_2$ at the corner, and $\Omega_1$ is the unbounded exterior domain. The refractive indices of the cylinder and the surrounding medium are $n_2$ and $n_1$, respectively. We consider the $H$-polarization so that the electric and magnetic fields are perpendicular and parallel to the $z$ axis, respectively.

The asymptotic theory for electromagnetic fields near edges of 2D wedges was first developed by Meixner in 1972 [4], and corrected by Andersen and Solodukhov in 1978 [13]. If the structure is illuminated by an incident wave with free space wavenumber $k_0$, the nonzero field components near the edge can be expanded as

$$H_z(\rho,\theta) = CA_z(\theta)\rho^{\tau} + \cdots, \quad (1)$$

$$E_\rho(\rho,\theta) = CA_\rho(\theta)\rho^{\tau-1} + \cdots, \quad (2)$$

$$E_\theta(\rho,\theta) = CA_\theta(\theta)\rho^{\tau-1} + \cdots, \quad (3)$$

where $H_z$ is the $z$ component of the magnetic field, $E_\rho$ and $E_\theta$ are the components of the electric field along the radial and angle directions, respectively, $\tau$ is the singularity exponent satisfying $\mathrm{Re}(\tau) \geq 0$, $A_z$, $A_\rho$ and $A_\theta$ are known functions of $\theta$, and $C$ is a coefficient that depends on the incident wave and the geometry of the structure.

If there are only two different media in the vicinity of the corner, such as the case shown in Fig. 1, then the exponent $\tau$ satisfies either

$$\tan\left[\tau\pi\frac{(1+\theta')}{2}\right] / \tan\left[\tau\pi\frac{(1-\theta')}{2}\right] = -\frac{n_2^2}{n_1^2}, \quad (4)$$

or

$$\tan\left[\tau\pi\frac{(1-\theta')}{2}\right] / \tan\left[\tau\pi\frac{(1+\theta')}{2}\right] = -\frac{n_2^2}{n_1^2}, \quad (5)$$

where $\theta' = 1 - 2\theta_1/\pi$ [14]. In general, Eqs. (4) and (5) have infinitely many complex solutions. If we denote the solution of Eq. (4) with the smallest real part by $\tau_+$, and the similar solution of Eq. (5) by $\tau_-$, then $\tau$ is either $\tau_+$ or $\tau_-$ whichever has the smaller real part.

It is known that $\tau$ satisfies $0 \leq \mathrm{Re}(\tau) < 1$, thus in general the transverse electric field components diverge as $\rho \to 0$. Since the coefficient $C$ is unknown for general cylindrical structures, the asymptotic theory does not give the actual field near the edge, thus numerical solutions are needed. To assess the accuracy of the numerical solutions, we reconstruct the exponent $\tau$ and compare it with the exact value for some test problems.

## 3. BOUNDARY INTEGRAL EQUATIONS

For scattering problems of penetrable cylinders, there are many boundary integral equation formulations [10, 11, 15–18]. Some of these formulations are proposed for high frequency problems where the size of the cylinder (i.e, its cross section) is much larger than the free space wavelength [19–21]. We are concerned with applications in plasmonics, where the sizes of the scatterers are often small compared with the wavelength, but the strong near-fields and the singular field behavior are highly important. Therefore, we choose to use one of the simplest BIE formulations and show that highly accurate numerical solutions can be obtained based on a graded mesh technique and proper discretization schemes.

For 2D problems and the $H$-polarization, the $z$ component of the magnetic field, denoted by $H_z$ or $u$, satisfies the following Helmholtz equation

$$\frac{\partial}{\partial x}\left(\frac{1}{n^2}\frac{\partial u}{\partial x}\right) + \frac{\partial}{\partial y}\left(\frac{1}{n^2}\frac{\partial u}{\partial y}\right) + k_0^2 u = 0, \quad (6)$$

where $\boldsymbol{r} = (x, y)$ and $n = n(\boldsymbol{r})$ is the refractive index function. In addition, we denote $u$ in $\Omega_2$ and $\Omega_1$ by $u_2$ and $u_1$, respectively. In the exterior domain $\Omega_1$, we specify an incident wave

$$u^{(i)}(\boldsymbol{r}) = e^{\mathrm{i}(\alpha x + \beta y)}, \quad (7)$$

where $\alpha = k_0 n_1 \cos[\theta^{(i)}]$, $\beta = k_0 n_1 \sin[\theta^{(i)}]$, and $\theta^{(i)}$ is the incident angle, i.e., the angle between the wavevector and the $x$ axis. Notice that $u_1 = u^{(i)} + u^{(s)}$, where $u^{(s)}$ is the scattered wave satisfying the Sommerfeld radiation condition at infinity.

Let $\Gamma$ be the common boundary of $\Omega_1$ and $\Omega_2$, and $\boldsymbol{\nu}$ be the unit normal vector of $\Gamma$ pointing into $\Omega_1$, our formulation involves boundary integral operators $\boldsymbol{S}_1$, $\boldsymbol{S}_2$, $\boldsymbol{K}_1$ and $\boldsymbol{K}_2$ defined by

$$(\boldsymbol{S}_j\psi)(\boldsymbol{r}) = 2\int_\Gamma G_j(\boldsymbol{r},\tilde{\boldsymbol{r}})\psi(\tilde{\boldsymbol{r}})\mathrm{d}s(\tilde{\boldsymbol{r}}), \tag{8}$$

$$(\boldsymbol{K}_j\psi)(\boldsymbol{r}) = 2\int_\Gamma \frac{\partial G_j(\boldsymbol{r},\tilde{\boldsymbol{r}})}{\partial \boldsymbol{\nu}(\tilde{\boldsymbol{r}})}\psi(\tilde{\boldsymbol{r}})\mathrm{d}s(\tilde{\boldsymbol{r}}), \tag{9}$$

for $\boldsymbol{r} \in \Gamma$ and $j = 1, 2$. In the above, $\psi$ is an arbitrary function defined on $\Gamma$, $G_j$ is the free space Green's function of the Helmholtz equation with wavenumber $k_0 n_j$, i.e.,

$$G_j(\boldsymbol{r},\tilde{\boldsymbol{r}}) = \frac{\mathrm{i}}{4}H_0^{(1)}(k_0 n_j|\boldsymbol{r}-\tilde{\boldsymbol{r}}|), \quad \boldsymbol{r} \neq \tilde{\boldsymbol{r}}, \tag{10}$$

where $H_0^{(1)}$ is the Hankel function of first kind and zeroth order.

For any $\boldsymbol{r} \in \Omega_2$, $u_2(\boldsymbol{r})$ is related to $u_2$ and $\partial_\nu u_2$ on boundary $\Gamma$ through Green's representation theorem. Taking the limit for $\boldsymbol{r}$ approaching a point on $\Gamma$, we obtain the following BIE for $u_2$ [22]:

$$\boldsymbol{K}_2 u_2 + \rho_2 u_2 = \boldsymbol{S}_2 \frac{\partial u_2}{\partial \boldsymbol{\nu}}, \tag{11}$$

where $\rho_2 = \rho_2(\boldsymbol{r})$ is the inner angle (in radian) of $\Omega_2$ at $\boldsymbol{r} \in \Gamma$ divided by $\pi$. Thus $\rho_2(\boldsymbol{r}) = 1$ if $\boldsymbol{r}$ is a smooth point of $\Gamma$. Notice that the unit normal vector is not defined at corner points. In addition, since $u$ is the $z$-component of magnetic field, $\partial_\nu u$ along $\Gamma$ is proportional to the tangential component of electric field. Therefore, near the corner, $\partial_\nu u_2$ has the same asymptotic behavior as $E_\rho$, and it blows up like $\rho^{\tau-1}$. To overcome this difficulty, we use two techniques. The first one is a graded mesh for discretizing $\Gamma$ [22, 23], and the second one is to replace $\partial_\nu u_2$ by a new function $\phi_2$ [24]. Let $\Gamma$ be given (in counterclockwise direction) by

$$\mathbf{r}(t) = (x(t), y(t)), \quad 0 \le t \le 1, \tag{12}$$

where $t = 0$ and $t = 1$ correspond to the same corner. The arc-length differential in the boundary integrals can be written as $\mathrm{d}s = |\boldsymbol{r}'(t)|\mathrm{d}t$, where $\boldsymbol{r}'(t)$ is the derivative of $\boldsymbol{r}(t)$ with respect to $t$. Assuming $|\boldsymbol{r}'(t)|$ approaches zero sufficiently fast as $t \to 0$ and $t \to 1$, we define function $\phi_2$ and operator $\tilde{\boldsymbol{S}}_2$ such that

$$\phi_2 = |\boldsymbol{r}'|\partial_\nu u_2, \quad \boldsymbol{S}_2 \partial_\nu u_2 = \tilde{\boldsymbol{S}}_2 \phi_2. \tag{13}$$

As a result, Eq. (11) becomes

$$\boldsymbol{K}_2 u_2 + \rho_2 u_2 = \tilde{\boldsymbol{S}}_2 \phi_2. \tag{14}$$

If the real part of the singularity exponent $\tau$ is positive, it is always possible to choose a parametric representation of $\Gamma$, such that $\phi_2$ is continuous and is zero at the corner point.

Similarly, a BIE for $u^{(s)}$ can be derived by taking the limit to $\Gamma$ from the Green's representation theorem of the Helmholtz equation in $\Omega_1$. We have

$$\boldsymbol{K}_1 u^{(s)} - \rho_1 u^{(s)} = \boldsymbol{S}_1 \frac{\partial u^{(s)}}{\partial \boldsymbol{\nu}}, \tag{15}$$

where $\rho_1 = \rho_1(\boldsymbol{r})$ is the outer angle of $\Omega_2$ at $\boldsymbol{r} \in \Gamma$ divided by $\pi$. With the defination of $\phi^{(s)}$ and $\tilde{\boldsymbol{S}}_1$ given by

$$\phi^{(s)} = |\boldsymbol{r}'|\partial_\nu u^{(s)}, \quad \boldsymbol{S}_1 \partial_\nu u^{(s)} = \tilde{\boldsymbol{S}}_1 \phi^{(s)}, \tag{16}$$

Eq. (15) becomes

$$\boldsymbol{K}_1 u^{(s)} - \rho_1 u^{(s)} = \tilde{\boldsymbol{S}}_1 \phi^{(s)}. \tag{17}$$

Since $u$ and $(1/n^2)\partial_\nu u$ are continuous on $\Gamma$, we can rewrite the BIE for $u^{(s)}$ and $\phi^{(s)}$ as an equation for $u_2$ and $\phi_2$. Therefore, we obtain the following system of BIEs

$$\begin{bmatrix} \tilde{\boldsymbol{S}}_2 & -\rho_2 - \boldsymbol{K}_2 \\ \eta\tilde{\boldsymbol{S}}_1 & \rho_1 - \boldsymbol{K}_1 \end{bmatrix} \begin{bmatrix} \phi_2 \\ u_2 \end{bmatrix} = \begin{bmatrix} 0 \\ R \end{bmatrix}, \tag{18}$$

where $\eta = (n_1/n_2)^2$, $\phi^{(i)} = |\boldsymbol{r}'|\partial_\nu u^{(i)}$, and

$$R = \tilde{\boldsymbol{S}}_1 \phi^{(i)} + (\rho_1 - \boldsymbol{K}_1) u^{(i)}. \tag{19}$$

The above approach based on $\phi_2$ (instead of $\partial_\nu u_2$) leads to more accurate numerical solutions, since the linear system resulting from the discretization of Eq. (18) is better balanced and has a smaller condition number.

## 4. DISCRETIZATION SCHEMES

The BIEs can be discretized by a uniform sampling of $t$ and approximating the integrals by quadrature rules. To obtain a graded mesh on the boundary $\Gamma$, the parametric representation (12) must be properly designed. If $\Gamma$ is given in its original representation with a parameter $w$ from $w = 0$ to $2\pi$, we can change $w$ to $t$ by the following transform [22, 23]:

$$w(t) = \frac{2\pi w_1^p}{w_1^p + w_2^p}, \quad 0 \le t \le 1, \tag{20}$$

where

$$w_1 = \frac{p-2}{2p}(2t-1)^3 + \frac{2t-1}{p} + \frac{1}{2}, \quad w_2 = 1 - w_1.$$

This transform depends on a parameter $p$. The derivatives of $w$, up to the $(p-1)$th order, vanish at $t = 0$ and $t = 1$. When it is used to discretize $\Gamma$ with a uniform sampling of $t$, more discretization points become concentrated near the corner with a larger value of the parameter $p$, while the discretization points remain well distributed away from the corner. Notice that the density of the discretization points near the corner may be fine tuned via a suitable choice of $p$.

When $t$ is discretized as $t_k = k/M$ for $k = 0, 1, ..., M$, the operators $\boldsymbol{K}_j$ and $\tilde{\boldsymbol{S}}_j$ are approximated by $M \times M$ matrices. Let $\boldsymbol{B}$ be a boundary integral operator given by

$$\varphi(\boldsymbol{r}) = \int_\Gamma B(\boldsymbol{r},\tilde{\boldsymbol{r}})\psi(\tilde{\boldsymbol{r}})\mathrm{d}s(\tilde{\boldsymbol{r}}), \quad \boldsymbol{r} \in \Gamma, \tag{21}$$

where $B(\boldsymbol{r},\tilde{\boldsymbol{r}})$ is the kernel and $\psi$ is an arbitrary function defined on $\Gamma$. Using the parametric representation (12), Eq. (21) becomes

$$\varphi(\boldsymbol{r}(t)) = \int_0^1 B(\boldsymbol{r}(t),\boldsymbol{r}(\tau))\psi(\boldsymbol{r}(\tau))\ |\boldsymbol{r}'(\tau)|\mathrm{d}\tau. \tag{22}$$

As a periodic function of $t$, $\psi(\boldsymbol{r}(t))$ can be approximated by its trigonometric interpolation [25]:

$$\psi(\boldsymbol{r}(t)) \approx \sum_{k=1}^{M} \psi_k \Psi(t - t_k), \tag{23}$$

where $\psi_k = \psi(\boldsymbol{r}(t_k))$ and $\Psi(t) = \sin(M\pi t)/[M\tan(\pi t)]$. This leads to

$$\varphi_l \approx \sum_{k=1}^{M} B_{lk}\psi_k, \quad l = 1, 2, ..., M, \tag{24}$$

where $\varphi_l = \varphi(\boldsymbol{r}(t_l))$, and

$$B_{lk} = \int_0^1 B(\boldsymbol{r}(t_l), \boldsymbol{r}(\tau))\Psi(\tau - t_k)\ |\boldsymbol{r}'(\tau)|\mathrm{d}\tau. \quad (25)$$

Therefore, $\boldsymbol{B}$ is approximated by a matrix with entries $B_{lk}$ for $1 \le l, k \le M$.

For operators $\tilde{\boldsymbol{S}}_1$ and $\tilde{\boldsymbol{S}}_2$, $|\boldsymbol{r}'|$ is combined with $\partial_\nu u$ to define the function $\phi$ as in Eqs. (13) and (16). Therefore, for a similarly defined operator $\tilde{\boldsymbol{B}}$, Eq. (24) becomes

$$\varphi_l \approx \sum_{k=1}^{M} \tilde{B}_{lk}\tilde{\psi}_k, \quad l = 1, 2, ..., M, \quad (26)$$

for $\tilde{\psi}_k = \psi(\boldsymbol{r}(t_k))|\boldsymbol{r}'(t_k)|$ and

$$\tilde{B}_{lk} = \int_0^1 B(\boldsymbol{r}(t_l), \boldsymbol{r}(\tau))\Psi(\tau - t_k)\mathrm{d}\tau. \quad (27)$$

Thus, $\tilde{\boldsymbol{B}}$ is approximated by the matrix with entries $\tilde{B}_{lk}$.

Since the operators $\boldsymbol{K}_j$, $\boldsymbol{S}_j$ or $\tilde{\boldsymbol{S}}_j$ have logarithmic singularities at $\boldsymbol{r} = \tilde{\boldsymbol{r}}$, we assume $\boldsymbol{B}$ also has a logarithmic singularity, and its kernel can be written as

$$B(\boldsymbol{r}(t), \boldsymbol{r}(\tau)) = B_1(t, \tau)\ln\{4\sin^2[\pi(t - \tau)]\} + B_2(t, \tau), \quad (28)$$

where $B_1$ and $B_2$ are smooth functions. The integrals involving $B_2$ can be evaluated by the standard trapezoidal rule, and the integrals involving $B_1$ and the logarithmic term can be evaluated by a special high order quadrature formula [22]. Therefore, approximations to $B_{lk}$ and $\tilde{B}_{lk}$ can be obtained. However, when the imaginary part of $k_0 L n_j$ is large, where $L$ is the diameter of $\Omega_2$, $B_1$ and $B_2$ can be very large, the above approach based on analytic splitting of the kernel suffers large cancellation errors. In that case, we prefer to use Alpert's hybrid Gauss-trapezoidal rule that takes care of the logarithmic singularity implicitly [26]. Although Alpert's method has a lower order of accuracy than the analytic kernel-splitting method, it is more robust and easier to implement.

Notice that $\rho_1$ and $\rho_2$ are discontinuous functions on $\Gamma$ with their values different from 1 only at the corner. An alternative formula for $\rho_2$ can be obtained from a BIE of the Laplace equation corresponding to Eq. (11) and evaluating the BIE on a constant solution. This leads to

$$\rho_2 = -\boldsymbol{K}_0 1, \quad \rho_1 = 2 - \rho_2 = 2 + \boldsymbol{K}_0 1, \quad (29)$$

where operator $\boldsymbol{K}_0$ is defined as in Eq. (9) with $G_j$ replace by the free space Green's function of the Laplace equation

$$G_0(\boldsymbol{r}, \boldsymbol{r}') = -\frac{1}{2\pi}\ln|\boldsymbol{r} - \boldsymbol{r}'|, \quad \boldsymbol{r} \neq \boldsymbol{r}',$$

and $\boldsymbol{K}_0 1$ is a function obtained by applying the operator $\boldsymbol{K}_0$ on constant function 1. It turns out that accuracy can be improved when $\rho_1$ and $\rho_2$ are evaluated from the above formulae with the same graded mesh and a consistent discretization scheme [22, 23].

In summary, the BIE system (18) is discretized as a $(2M) \times (2M)$ linear system, where $\phi_2$ and $u_2$ are approximated by column vectors of length $M$, $\boldsymbol{K}_1$, $\boldsymbol{K}_2$, $\tilde{\boldsymbol{S}}_1$ and $\tilde{\boldsymbol{S}}_2$ are approximated by $M \times M$ matrices, $\rho_1$ and $\rho_2$ are approximated by vectors and rewritten as diagonal matrices for the linear system.

## 5. NUMERICAL RESULTS

In this section, we present numerical results for the two cylinders shown in Fig. 1, assuming the material of the cylinders is gold, the surrounding medium is air, and the wavelength of the incident wave is $\lambda = 1\mu m$. The refractive indices of gold and air are assumed to be $n_2 = 0.22769 + \mathrm{i}6.4731$ and $n_1 = 1$, respectively.

For the drop-shaped cylinder shown in Fig. 1(a), the boundary $\Gamma$ is given by

$$x(t) = L\sin[0.5w(t)], \quad y(t) = -S\sin[w(t)], \quad (30)$$

where $w(t)$ is given in Eq. (20), $L = 0.2\mu m$ is the horizontal width of the structure, $2\theta_1 = \pi/3$ is the inner angle, and $S = 0.5L\tan\theta_1$. For the singularity exponent of this structure, we solve Eqs. (4) and (5) and obtain

$$\tau_+ = 0.5705755 - \mathrm{i}0.002184, \ \tau_- = 1.20665 + \mathrm{i}0.0004715. \quad (31)$$

The definition of $C$ depends on the scaling for $A_z$, $A_\rho$ and $A_\theta$ in Eqs. (1), (2) and (3). Since $\partial_\nu u$ is proportional to $E_\rho$, we assume the scaling is such that the leading term of $\partial_\nu u_2$ on $\Gamma$ is exactly $C\rho^{\tau-1}$, where $\rho$ is the distance to the corner point.

Numerical solutions are calculated using a graded mesh with $p = 7$ and a total of $M = 550$ discretization points. The integrals in Eqs. (25) and (27) are evaluated using the explicit kernel-splitting approach. In Fig. 2, we show $|\partial_\nu u_2|$ along the

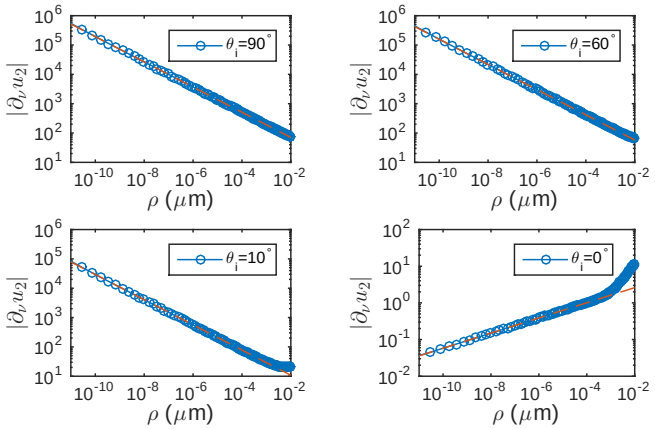


**Fig. 2.** Cylinder with cross section shown in Fig. 1(a): magnitude of $\partial_\nu u_2$ along boundary $\Gamma$ in the vicinity of the corner for a few different incident angles.

boundary $\Gamma$ as a function of $\rho$. The four plots in Fig. 2 correspond to plane incident waves, given in Eq. (7), with incident angles $\theta^{(i)} = 90°$, $60°$, $10°$ and $0°$, respectively. To calculate the exponent $\tau$ and coefficient $C$, we use a least squares method based on those discretization points with $\rho \in [10^{-10}, 10^{-4}]\mu m$. The results are listed in Table 1 for a few different incident angles. In addition, we show $|C\rho^{\tau-1}|$ in Fig. 2 as the red dashed lines.

According to the asymptotic theory [4, 13], the singularity exponent should be $\tau = \tau_+$, since $\mathrm{Re}(\tau_+)$ is less than $\mathrm{Re}(\tau_-)$. This is confirmed by the numerical results listed in Table 1 for incident angle $\theta^{(i)} \neq 0°$. Notice that the structure under consideration is symmetric with respect to the $x$-axis. It turns out that the leading asymptotic term is an odd function of $y$, and thus it cannot be excited by a horizontal plane wave (i.e., $\theta^{(i)} = 0°$). The results shown in Table 1 indicate that $\tau$ becomes $\tau_-$ when

**Table 1.** Cylinder with cross section shown in Fig. 1(a): singularity exponent $\tau$ and leading coefficient $C$ obtained from numerical solutions for a few different incident angles.

| angle $\theta^{(i)}$ | exponent $\tau$ | coefficient $C$ |
|---|---|---|
| 90° | 0.5705 - i0.00218 | 2.600 - i9.431 |
| 60° | 0.5705 - i0.00221 | 3.193 - i7.345 |
| 30° | 0.5706 - i0.00231 | 2.124 - i3.837 |
| 10° | 0.5710 - i0.00265 | 0.7588 - i1.296 |
| 5° | 0.5715 - i0.00313 | 0.3799 - i0.6573 |
| 0° | 1.2066 + i0.00679 | -0.9620 - i6.674 |

$\theta^{(i)} = 0°$. We notice that the numerically constructed $\tau$ is most accurate for $\theta^{(i)} = 90°$, and the accuracy decreases as $\theta^{(i)}$ is decreased. This does not mean that our numerical solutions are less accurate when $\theta^{(i)}$ moves away from 90°. In fact, when $\theta^{(i)}$ decreases from 90° to 0°, the magnitude of $C$ decreases, the leading term with exponent $\tau_+$ becomes less dominant, other terms including the term with exponent $\tau_-$, become more important, thus the numerically constructed $\tau$ has less number of correct digits. However, in all cases, we obtain at least two correct digits in $\tau$. Since the magnitude of $C$ is largest for $\theta^{(i)} = 90°$, we conclude that local field is strongest when the propagation direction of the incident plane wave is perpendicular to the bisector of the structure.

The second example is again a gold cylinder but with a cross section shown in Fig. 1(b). The boundary $\Gamma$ is given by

$$x(t) = L\sin\left[1.5w(t)\right], \quad y(t) = S\sin\left[w(t)\right] \tag{32}$$

for the same $w(t)$, where $L = 1\mu m$, $2\theta_1 = 5\pi/3$, and $S = 3L/2 \cdot \tan(\pi - \theta_1)$. Near the corner, this structure can be considered as the first structure shown in Fig. 1(a) with two media interchanged. Therefore, the values of $\tau_+$ and $\tau_-$ can be simply obtained by swapping those given in Eq. (31), i.e.,

$$\tau_+ = 1.20665 + \text{i}0.0004715, \ \tau_- = 0.5705755 - \text{i}0.002184. \tag{33}$$

As a result, the singularity exponent $\tau$ should be $\tau_-$ above.

Notice that the horizontal width $L$ of this structure is much larger than the first one. Since the imaginary part of $k_0 L n_2 \approx 1.43 + \text{i}40.7$ is quite large, the quadrature scheme based on explicit kernel-splittings becomes inaccurate. Therefore, we turn to Alpert's hybrid Gauss-trapezoidal method. The BIEs are discretized using a graded mesh for $p = 7$ and $M = 124$ points. The involved integrals are evaluated by Alpert's second order method.

In Fig. 3, we show $|\partial_\nu u_2|$ along the boundary $\Gamma$ for a few different incident waves. To find the exponent $\tau$ and coefficient $C$ numerically, we again use a least squares method based on those points with $\rho \in [10^{-10}, 10^{-4}]\mu m$. There are only 12 points in this range, but the numerically constructed $\tau$ still have at least two correct digits as shown in Table 2. For this structure, the leading asymptotic term corresponds to the $\tau_-$ given in Eq. (33), and is an even function of $y$. Therefore, it can be excited by a horizontal incident wave, as indicated by the results for $\theta^{(i)} = 180°$. The leading term can also be excited by a vertical incident wave, since structure is not symmetric with respect to the $y$-axis. The numerical results on coefficient $C$ indicate

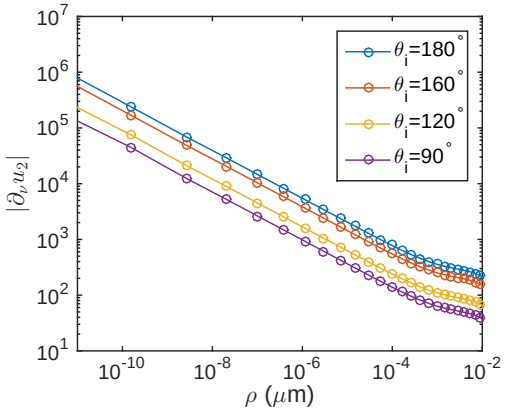


**Fig. 3.** Cylinder with cross section shown in Fig. 1(b): the magnitude of $\partial_\nu u_2$ along boundary $\Gamma$ in the vicinity of the corner for a few different incident angles.

**Table 2.** Cylinder with cross section shown in Fig. 1(b): singularity exponent $\tau$ and leading coefficient $C$ obtained from numerical solutions for a few different incident angles.

| angle $\theta^{(i)}$ | exponent $\tau$ | coefficient $C$ |
|---|---|---|
| 90° | 0.5692 - i0.0015 | 0.240 - i2.55 |
| 120° | 0.5708 - i0.0020 | -0.993 + i4.38 |
| 160° | 0.5713 - i0.0031 | 8.56 + i5.85 |
| 180° | 0.5714 - i0.0022 | 13.1 + i6.78 |

that the field near the corner is strongest when $\theta^{(i)} = 180°$, i.e., when the incident wave propagates toward the structure along its bisector.

## 6. CONCLUSION

For applications in nanophotonics, it is important to calculate the local fields for subwavelength resonators such as metallic nanoparticles. Due to the possible singularities, geometric features such as sharp corners and edges greatly influence the local fields. For 2D structures, an asymptotic theory for electromagnetic fields near sharp edges is available [4, 13], but in general the leading coefficients are still unknown. To capture the singular field behavior near corners and edges, it is usually necessary to use special numerical methods involving basis functions with the exact singularity exponents [6]. In this paper, we develop a purely numerical BIE method that can reconstruct the singularity exponents and calculate the leading coefficients. In all cases, the calculated exponents have at least two correct significant digits, indicating that the numerical solutions are accurate.

Our BIE method relies on a graded mesh technique and a rescaling for unknown functions that exhibit singular behaviors. The BIEs are discretized using two different quadrature methods. The first one uses explicit kernel splittings and is highly accurate for dielectric structures and small metallic structures. The second one is Alpert's hybrid Gauss-trapezoidal rule which is also accurate and not subject to any restrictions on the size of the structures. The current study indicates that our newly formulated BIE method is particularly effective for analyzing 2D

structures with field singularities. Furthermore, the method can be combined with a one-dimensional mode expansion method [27, 28] to solve three-dimensional scattering problems for cylindrical structures with sharp corners and edges.

## FUNDING

China Postdoctoral Science Foundation (2016M600903), National Natural Science Foundation of China (U1530401), Research Grants Council of Hong Kong Special Administrative Region, China (CityU 11301914).

## REFERENCES

1. S. A. Maier, *Plasmonics: Fundamentals and Applications* (New York, Springer, 2007).
2. M. Pelton and G. Bryant, *Introduction to Metal-Nanoparticle Plasmonics* (Hoboken, New Jersey, Wiley, 2013).
3. S. Kühn, U. Håkanson, L. Rogobete, and V. Sandoghdar, "Enhancement of single-molecule fluorescence using a gold nanoparticle as an optical nanoantenna," Phys. Rev. Lett., **97**: 017402 (2006).
4. J. Meixner, "The behavior of electromagnetic fields at edges," IEEE Transactions on Antennas and Propagation, **20**(4): 442–446 (1972).
5. R. D. Graglia, A. F. Peterson, L. Matekovits, and P. Petrini, "Singular hierarchical curl-conforming vector basis functions for triangular cells," IEEE Transactions on Antennas and Propagation, **62**: 3632–3644 (2014).
6. A. F. Peterson and R. D. Graglia, "Basis functions for vertex, edge, and corner singularities: a review," IEEE Journal on Multiscale and Multiphysics Computational Techniques, **1**: 161–175 (2016).
7. T. Lu and D. Yevick, "Comparative evaluation of a novel series approximation for electromagnetic fields at dielectric corners with boundary element method applications," J. Lightwave Technol. **22**: 1426–1432 (2004).
8. M. M. Bibby, A. F. Peterson, and C. M. Coldwell, "High order representations for singular currents at corners," IEEE Transactions on Antennas and Propagation, **56**(8): 2277–2287 (2008).
9. M. M. Bibby and A. F. Peterson, "High-order treatment of junctions and edge singularities with the locally-corrected Nyström method," ACES Journal, **28**(10): 892–902 (2013).
10. E. Marx, "Computed fields near the edge of a dielectric wedge," IEEE Transactions on Antennas and Propagation, **38**(9): 1438–1442 (1990).
11. E. Marx, "Electromagnetic scattering from a dielectric wedge and the single hypersingular integral equation," IEEE transactions on antennas and propagation, **41**(8): 1001–1008 (1993).
12. M. R. Disfani, M. S. Abrishamian, and P. Berini, "Electromagnetic fields near plasmonic wedges," Opt. Lett., **37**(10): 1667–1669 (2012).
13. J. B. Andersen and V. V. Solodukhov, "Field behavior near a dielectric wedge," IEEE Transactions on Antennas and Propagation, **26**(4): 598–602 (1978).
14. L. Li, "Field singularities at lossless metal-dielectric arbitrary-angle edges and their ramifications to the numerical modeling of gratings," J. Opt. Soc. Am. A, **29**(4): 593–604 (2012).
15. R. Kress and G. F. Roach, "Transmission problems for the Helmholtz equation," Journal of Mathematical Physics, **19**(6): 1433–1437 (1978).
16. M. Costabel and E. Stephan, "A direct boundary integral equation method for transmission problems," Journal of Mathematical Analysis and Applications, **106**(2): 367–413 (1985).
17. R. E. Kleinman and P. A. Martin, "On single integral equations for the transmission problem of acoustics," SIAM Journal on Applied Mathematics, **48**(2): 307–325 (1988).
18. Y. Boubendir, V. Domínguez, D. Levadoux, and C. Turc, "Regularized combined field integral equations for acoustic transmission problems," SIAM Journal on Applied Mathematics, **75**(3): 929–952 (2015).
19. P. G. Martinsson and V. Rokhlin, "A fast direct solver for boundary integral equations in two dimensions," Journal of Computational Physics, **205**(1): 1–23 (2005).
20. J. Helsing and R. Ojala, "Corner singularities for elliptic problems: Integral equations, graded meshes, quadrature, and compressed inverse preconditioning," Journal of Computational Physics, **227**(20): 8820–8840 (2008).
21. J. Helsing and A. Karlsson, "An accurate boundary value problem solver applied to scattering from cylinders with corners," IEEE Transactions on Antennas and Propagation, **61**(7): 3693–3700 (2013).
22. D. Colton and R. Kress, *Inverse acoustic and electromagnetic scattering theory*, 3rd ed. (New York, Springer, 2013).
23. R. Kress, "A Nyström method for boundary integral equations in domains with corners," Numer. Math. **58**(1): 145–161 (1990).
24. W. Lu and Y. Y. Lu, "Waveguide mode solver based on Neumann-to-Dirichlet operators and boundary integral equations," Journal of Computational Physics, **231**(4): 1360–1371 (2012).
25. L. N. Trefethen, *Spectral Methods in MATLAB* (Philadelphia, SIAM, 2000).
26. B. K. Alpert, "Hybrid gauss-trapezoidal quadrature rules," SIAM Journal on Scientific Computing, **20**(5): 1551–1584 (1999).
27. H. Shi and Y. Y. Lu, "Efficient vertical mode expansion method for scattering by arbitrary layered cylindrical structures," Opt. Express, **23**(11): 14618–14629 (2015).
28. H. Shi, X. Lu, and Y. Y. Lu, "Vertical mode expansion method for numerical modeling of biperiodic structures," J. Opt. Soc. Am. A, **33**(5): 836–844 (2016).